J Mater Sci (2007) 42:8071–8082
DOI 10.1007/s10853-007-1915-0

# Diffusion-limited reactive wetting: effect of interfacial reaction behind the advancing triple line

**F. Hodaj · O. Dezellus · J. N. Barbier · A. Mortensen · N. Eustathopoulos**

Received: 28 March 2007 / Accepted: 4 June 2007 / Published online: 3 July 2007


**Abstract** Using the "dispensed drop" variant of the sessile drop technique, spreading kinetics of dilute Cu–Cr alloys on smooth vitreous carbon substrates are measured under helium microleak conditions. In this system, it is known that the drop spreading rate is controlled by diffusion of the reactive atom species (Cr) from the bulk liquid to the triple line, where wetting is induced by formation of an interfacial layer of chromium carbide. Microstructural characterization of rapidly cooled drops shows that growth of the interfacial reaction product layer continues behind the moving solid–liquid–vapor triple line. The spreading velocity is modeled by finite-difference numerical analysis of diffusion near the triple line in the presence of continued interfacial reaction, simplifying the growth rate as being constant and using realistic parameter values. We show that continued interfacial reaction explains the dependence of the triple line spreading rate on the instantaneous wetting angle that is observed in this system.

F. Hodaj (✉) · J. N. Barbier · N. Eustathopoulos
SIMAP – UMR CNRS 5266, INP Grenoble-UJF, Domaine Universitaire, BP 75 – 1130, rue de la Piscine, 38402 Saint Martin d'Heres, Cedex, France
e-mail: fhodaj@ltpcm.inpg.fr

O. Dezellus
LMI – UMR CNRS No. 5615, Université Claude Bernard Lyon 1, 43 Bd du 11 novembre 1918, 69622 Villeurbanne Cedex, France

A. Mortensen
Laboratory for Mechanical Metallurgy, Ecole Polytechnique Fédérale de Lausanne, Lausanne 1015, Switzerland

## Introduction

Non-metallic solids, such as oxides, carbides, or carbon, are generally poorly wetted by liquid engineering metals such as tin or copper: contact angles typically exceed 90° [1, 2]. The complications this produces in materials processes such as infiltration or brazing have motivated the search for various means to lower the contact angle in such systems.

One approach to this end is to alloy the metal with elements that, by reaction with the solid, form a better-wetted compound. On substrates of carbon for example, chromium or titanium alloyed into molten copper form, by reaction with the carbon, a chromium or titanium carbide. These carbides, of partly metallic character, are relatively well wetted by the metal [3, 4].

When a droplet of such reactive alloys comes in contact with the solid, it first spreads very rapidly, at a rate determined by the (low) viscosity of the metal. It thus quickly reaches a first metastable equilibrium contact angle, characteristic of the metal on the unreacted solid substrate. After a short transient stage (a few seconds) a thin continuous reaction layer is then formed along the solid/liquid interface [5]. Thereafter, since the reaction layer is better wetted than the original substrate, the drop starts spreading again as the layer expands outward of the triple line, parallel to the interface. In this second spreading process, the drop spreading rate is controlled, not by the metal viscosity, but rather by the rate at which the reaction product layer can grow at the triple line, parallel to the solid surface. Spreading continues in this manner until the contact angle becomes equal to the equilibrium contact angle of the alloy on the reaction product, $\theta_e$. Following this, the drop remains stable even though the reaction layer may continue to grow, both in thickness and further outwards of the triple line, along the substrate free surface.

In such systems, the rate at which the liquid spreads over the solid substrate after reaching its first metastable contact angle value is controlled by the rate at which the better-wetted interfacial reaction product grows parallel to the interface at the liquid/solid/vapor triple line. This, in turn, is generally governed either by (i) the local reaction kinetics at the triple line (an example is found in Refs. [5, 6]), or by (ii) the rate of supply of the active solute species to the triple line. Given the high diffusivity characteristic of liquids, it is by diffusion through the liquid (and not the solid nor the atmosphere) that reactive species are supplied from the bulk liquid to the triple line.

For diffusion-controlled spreading of a liquid drop over a flat solid substrate, a relatively simple analysis that assumes the interfacial reaction to be strictly localized at the triple line shows that the velocity of a sessile drop triple line $V = \mathrm{d}R/\mathrm{d}t$ (where $R$ is the radius of the drop base and $t$ is time) varies in direct linear proportion to the instantaneous contact angle $\theta$ [7] until $\theta$ reaches its equilibrium value over the reaction layer, $\theta_e$, at which point spreading stops:

$$\frac{\mathrm{d}R}{\mathrm{d}t} = \frac{2DF_{(t)}}{en_v}(C_o - C_e)\theta, \quad \theta > \theta_e \tag{1a}$$

$$\frac{\mathrm{d}R}{\mathrm{d}t} = 0, \quad \theta = \theta_e. \tag{1b}$$

Here, $D$ is the diffusion coefficient in the liquid phase, $n_v$ is the number of moles of reactive solute per unit volume of the reaction product, $e$ is the reaction product thickness at the triple line, $C_o$ is the nominal (far-field) drop reactive solute concentration, $C_e$ is the concentration of reactive solute in equilibrium with the reaction product (such that $C = C_e$ at the triple line). $F_{(t)}$ is strictly a function of time but in fact varies so little that it can be taken to be constant, remaining near 0.04 in usual sessile drop experiments [7].

When confronted with experiment, this relation shows good agreement with data for the spreading of Cu–Sn–Ti on vitreous carbon ($C_v$) near 1,100 °C for $\theta < 90°$ : the rate of spreading is indeed directly proportional to $\theta$, and the constant of proportionality agrees with that in Eq. 1a [4]. When compared with spreading kinetics measured for Cu–Cr alloy sessile drops on vitreous carbon, still for $\theta < 90°$, a direct linear relationship between $\mathrm{d}R/\mathrm{d}t$ and $\theta$ is again found, the slope of the line being again in accordance with Eq. 1a; however, the intercept of the line giving $\mathrm{d}R/\mathrm{d}t$ vs. $\theta$ with the $\theta$ axis is not at the origin ($\theta = 0$), but rather at a finite angle near 40° [3] as shown in Fig. 1.

This discrepancy was attributed to the presence of additional drop/substrate chemical reaction along the interface *behind* the triple line, causing solute also to be consumed along the liquid/solid interface. As a result, it

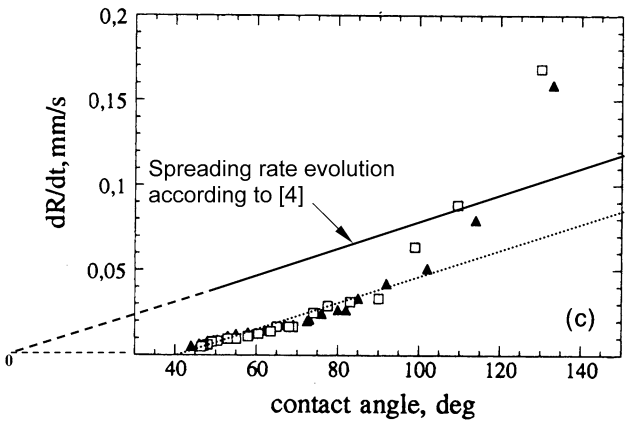


**Fig. 1** Experimental triple line velocity as a function of instantaneous contact angle $\theta$ for Cu–1 at.% Cr on vitreous carbon at 1,150 °C [3] and spreading rate according to Eq. 1a, Ref. [7]

was argued, a portion of the total flux of solute from the bulk of the drop is diverted from the triple line, reducing the flux that serves to drive drop spreading.

This interpretation was suggested by the following observations:

(i) Final measured chromium carbide interfacial reaction layers were relatively thick in the Cu–Cr/C system (several micrometers) and continued to thicken if the drop was held at temperature. By comparison, the TiC reaction layer that forms when Cu–Sn–Ti spreads on vitreous carbon ($C_v$) is known to be more impervious to diffusion, thus preventing continued reaction once it forms a continuous layer. The TiC reaction layer was indeed found to be much thinner than the chromium carbide layers formed in the Cu–Cr/C system [3, 4], and this system indeed obeys Eq. 1a.

(ii) A simple analytical calculation for the extreme case of kinetically unhindered chemical reaction with very fast diffusion of the reactive species through the reaction layer behind the triple line did, indeed, essentially result in a simple horizontal translation of the line linking $\mathrm{d}R/\mathrm{d}t$ with $\theta$ [3]. The shift was, however, unrealistically large, obviously as a result of the extreme assumption made in this calculation. We give here a quantitative demonstration that the interpretation offered earlier is indeed correct. Specifically we show, using the Cu–1.5% Cr/C system at 1,150 °C as a case study, that continued interfacial reaction behind the triple line indeed causes a horizontal translation of the straight line linking the triple line velocity with the instantaneous contact angle in diffusion-controlled reactive wetting. Interfacial reaction behind the triple line then effectively replaces $\theta$ in Eq. 1a with $(\theta–\theta_d)$, where $\theta_d$ is an essentially constant "dead angle" from

which diffusing solute is diverted away from the triple line to the interface.

We first present a set of new experimental results for Cu–1.50% Cr spreading on vitreous carbon at 1,150 °C, obtained using the dispensed drop method [5] (as opposed to the transferred drop technique used in Ref. [3]). We then present a numerical analysis of reactive spreading in this system that takes into account the influence of solid state diffusion through the reaction layer behind the triple line. Finally, we compare predictions with the data to show the existence of such a dead angle and to explore its dependence on interfacial reaction kinetics.

## Experimental

### Experimental procedures

Vitreous carbon ($C_v$) substrates were used. These feature no open porosity, an ash content less than 50 ppm and, after polishing, an average surface roughness of 2 nm. Before the experiments, all substrates were ultrasonically cleaned in acetone and then annealed. Wetting was studied using the dispensed drop method (a variant of the classical sessile drop technique), in a metallic furnace under a $10^{-3}$ Pa helium microleak atmosphere [5]. The copper–chromium alloys were prepared from pure Cu (99.999 wt.%) and Cr (99.3 wt.%), by in-situ melting and alloying in an alumina crucible during experiments, also under He microleak conditions ($10^{-3}$ Pa).

In the "dispensed drop" technique used here, the pre-alloyed metal is extruded through a small hole at the bottom of the alumina crucible, which is then lowered to effect contact of the metal with the substrate. The drop is then detached from the crucible by raising the latter. Spreading of the isolated drop is recorded using a video camera connected to a computer equipped with image analysis software for calculation of (i) the drop/substrate contact circle radius, $R$, with a precision of 2%, and (ii) the contact angle, $\theta$, with a precision of 2°, both as a function of time, $t$. In selected experiments, the drop was cooled rapidly by turning off the furnace power supply a few seconds after capillary equilibrium was reached. In the He microleak condition ($10^{-3}$ Pa) of the experiments, the cooling rate was about 3 K $s^{-1}$.

After cooldown the specimens were cut, embedded in resin, and polished for microstructural characterization. The interfacial reaction product chemistry and morphology were characterized by scanning electron microscopy.

### Experimental results

Four experiments were performed during the present study with Cu–1.5 at.% Cr at 1,150 °C, the drop volume varying from 1 to 9 $mm^3$. A typical plot of the variations in time of the contact angle $\theta$ and the droplet base radius $R$ is given in Fig. 2. In agreement with experimental results obtained using the transferred drop method [3], the Cu–1.5 at.% Cr alloy wets vitreous carbon well, the final contact angle being as low as 30°. Moreover, the $R(t)$ curve displays a time-dependent spreading rate $dR/dt$, indicating that local interfacial reaction kinetics do not govern the rate of spreading (e.g., [5, 6]).

Deducing from these data the triple line velocity $dR/dt$ and plotting this quantity as a function of the instantaneous contact angle $\theta$, one obtains the curve in Fig. 3 (plotted data are for spreading after complete transfer of the drop—i.e., for $\theta$ lower than 140°). As was observed in Ref. [3], when $\theta < 90°$ the data points lie roughly along a straight line that cuts the $\theta$-axis at a finite angle. This angle is, as in Ref. [3], near the final equilibrium contact angle $\theta_f = 30°$, characteristic of the liquid alloy at rest on the reaction product layer.

A cross-section of the interfacial region at the center of the droplet is shown in Fig. 4. In this experiment, rapid cooling of the sample was initiated after spreading, such that solidification of the alloy was achieved about 20 s later. A continuous chromium carbide reaction layer is visible along the whole interface. Chemical interaction between Cu–Cr liquid alloys and vitreous carbon can lead to the formation of two different carbides: $Cr_7C_3$ and $Cr_3C_2$. SEM characterization and microprobe analysis of the interfacial layers led to identification of the compound $Cr_7C_3$ rather than $Cr_3C_2$.

The thickness of carbide layer is around 2 μm at the center of the drop and decreases progressively to about 1 μm at the triple line, indicating that carbide growth kinetics are extremely rapid in this system. For this reason, it is very difficult to measure the real reaction layer thickness near the triple line as well as its gradient behind

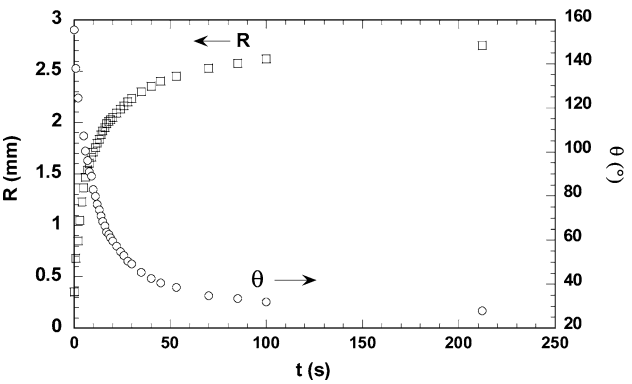


**Fig. 2** Drop base radius and contact angle evolution with time during spreading of Cu–1.5 at.% Cr on vitreous carbon at 1,150 °C using the dispensed drop method. The drop volume is 9 $mm^3$

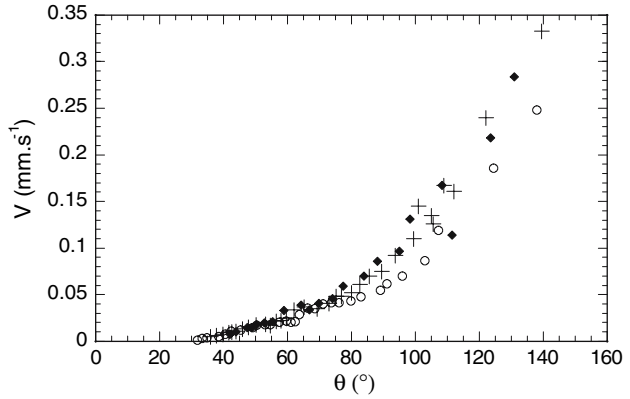


**Fig. 3** Triple line velocity as a function of instantaneous contact angle $\theta$ for Cu–1.50 at.% Cr alloy on vitreous carbon at 1,150 °C; three sets of data are included to show the reproducibility of the data and their size-independence: data for drops 1 $mm^3$ (♦); 3 $mm^3$ (+) and 9 $mm^3$ in volume (○)


**Fig. 4** Scanning electron micrograph of a cross-section through a drop of Cu–1.50 at.% $Cr/C_v$ interface at the center of the drop after spreading at 1,150 °C on vitreous carbon followed by rapid cooling (about 3 K/s)

the triple line by "post-mortem" examination because the observed reaction layer is thicker than it was during spreading. Therefore, the measured "post-mortem" thickness gradient is likely to be *lower* than it was during spreading, since during cooldown a greater amount of reaction layer thickening is expected where the reaction layer was thinner, i.e., near the triple line (this point will be discussed in greater detail in the next section—see Fig. 5). Still, these experimental results show that reaction takes place both at, and behind, the triple line during drop spreading in this system. Solute flux lines from the drop bulk therefore do not all converge to the triple line, since the interface now represents a second solute sink. We analyze this diffusion problem in what follows.

## Analysis

### General description

Consider a moving wetting front of a liquid binary alloy A–B, component B of which reacts with the solid substrate to form a solid reaction product. We assume that the reaction between B and the substrate is rapid upon initial contact of the liquid with the solid, causing the formation of a small thickness $e_a$ of reaction product at the triple line. Thereafter, reaction continues behind the triple line, leading to a gradual further increase in the thickness $e$ of the interfacial reaction layer, as shown in Fig. 5a.

Figure 5c presents a schematic evolution of the reaction layer profile during spreading when a decrease $\Delta\theta$ in the contact angle $\theta$ occurs after time $\Delta t$. This figure shows that the increase $\Delta e$ in the reaction layer thickness $e$ at any point along the interface depends on the distance from the triple line. As a result, the reaction layer thickness profile is not constant during spreading: it depends on time and also on the distance from the triple line.

The most reasonable assumption from a physical standpoint is that thickening of the reaction layer obeys a parabolic law corresponding to a growth rate controlled by diffusion through the layer. A corollary of a parabolic growth law is that, at any position along the interface, the relative increment in reaction layer thickness for a given increment of contact time $\Delta t$, $\Delta e/e$, becomes gradually smaller as one moves from the triple line to the drop axis, as depicted in Fig. 5c. For tractability of the moving boundary problem at hand, we simplify this "real situation" (Fig. 5c) by assuming that the reaction layer thickness profile is composed of two zones, namely (i) a region of constant thickness, $e_b$, extending from the center of the drop to within a certain distance $L$ from the triple line and (ii) an outer ring that extends from this point to the triple line where the reaction layer thickness is assumed to decrease linearly from $e_b$ down to its value at the triple line, $e_a$, as sketched in Fig. 5d.

### Calculation method

The rate of spreading of the liquid is governed by the rate at which the thin continuous solid reaction product layer grows at the moving triple line to reach an initial thickness $e_a$. We assume that the rate of growth of the reaction product at the triple line is limited by diffusive transport of solute element B through the liquid to the triple line. The local solute concentration along the triple line then equals the equilibrium concentration, $C_e$, in an A–B alloy contacting both the reaction product and the unreacted solid substrate at the temperature of the experiment.

We assume that spreading is isothermal, and that the liquid drop is sufficiently large for its bulk to be treated as an infinite medium having a constant solute concentration $C_o$. We neglect all curvature along the liquid/solid interface and thus model the liquid region near the triple line as a straight wedge of angle $\theta$.

In the liquid, solute can be transported by convection and diffusion. We assume, as was justified in Ref. [7], that in the

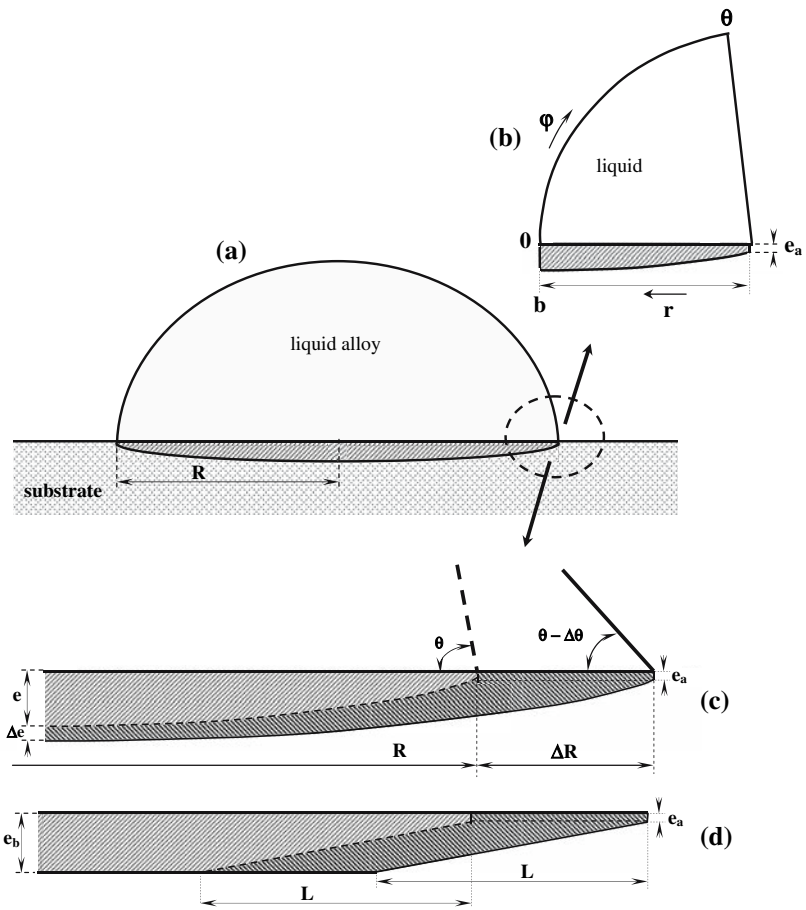


**Fig. 5** (**a**) Schematic illustration of reaction layer formation during spreading of a liquid alloy on a substrate at the liquid/solid interface. (**b**) Details of the zone near the triple line giving coordinates used in analysis. (**c**) Schematic evolution of the interfacial layer profile when a decrease $\Delta\theta$ in the contact angle $\theta$ occurs during spreading. (**d**) Assumed profile of the layer in analysis

immediate vicinity of the triple line diffusion is the dominating mechanism for solute transport. We therefore neglect the influence of convection in this region. As discussed in Ref. [7], this assumption is justified in practical situations.

It was also shown in Ref. [7] that, because of its cylindrical symmetry, this diffusion problem may be analyzed as a steady-state diffusion problem despite its intrinsically transient nature. It is then governed by the Laplace equation instead of Fick's law.

The volume considered is thus a straight wedge of angle $\theta$ extending in cylindrical coordinates $(r, \varphi)$ between radius $r = a$, situated at the triple line, and radius $r = b = a\exp(1/(2F_{(t)})) \gg a$ marking the (assumed sharp) boundary between the region where solute transport is by diffusion only, and the bulk liquid where convection keeps the liquid composition uniform at $C_o$, see Figs. 5b, 6a. Within the wedge the solute concentration $C$ obeys:

$$\nabla^2 C = \frac{1}{r}\frac{\partial C}{\partial r} + \frac{\partial^2 C}{\partial r^2} + \frac{1}{r^2}\frac{\partial^2 C}{\partial \varphi^2} = 0 \tag{2}$$

subject to boundary conditions:

$$\text{at } r = a,\ 0 \le \varphi \le \theta;\ C = C_e \tag{3}$$

$$\text{at } r = b,\ 0 \le \varphi \le \theta;\ C = C_0 \tag{4}$$

$$\text{at } \varphi = 0,\ a \le r \le b;\ D\frac{\partial C}{r\partial \varphi} = k\frac{de}{dt} = kV\frac{de}{dr} \tag{5}$$

$$\text{at } \varphi = \theta(t),\ a \le r \le b;\ \frac{\partial C}{\partial \varphi} = 0 \tag{6}$$

where $D$ is the solute diffusion coefficient in the liquid, $k$ is the (reaction-specific) constant of proportionality between the normal solute flux along the liquid/solid interface in the liquid and the rate of interfacial reaction product growth. The no-flux condition along the liquid surface (Eq. 6) implicitly assumes that there is no evaporation/condensation solute transfer between liquid and vapor phases.

The rate of motion of the triple line, $V = dR/dt$, is given explicitly by a simple mass balance stating that the flux of reactive solute supplied at the triple line at $r = a$ is fully used for radial extension of the wetted reaction layer—and hence of the drop contact area with the solid:

$$\int_0^{\theta} D\left(\frac{\partial C}{\partial r}\right)_{r=a} a\,d\varphi = n_v e_a \frac{dR}{dt} \tag{7}$$

where $e_a$ is the thickness of product reaction layer formed at the triple line, $n_v$ the mole number of reactive solute per unit volume of reaction product, and $R$ the radius of the liquid/substrate contact area.

## Solution method

The diffusion problem defined by Eqs. 2– 6 is most conveniently solved using the method of conjugate variables [8], as was done in Ref. [3] for an analogous problem. For the present calculations, we leave variable $\varphi$ unchanged and define dimensionless variables:

$$\eta = \ln\left(\frac{r}{a}\right) \tag{8}$$

$$\chi = \frac{C - C_e}{C - C_0} \tag{9}$$

Eq. 2 then becomes:

$$\frac{\partial^2 \chi}{\partial \eta^2} + \frac{\partial^2 \chi}{\partial \varphi^2} = 0 \tag{10}$$

such that the problem is recast into a diffusion problem on a rectangle, as illustrated in Fig. 6. When discretized using the finite-difference method, variable $\eta$ conveniently refines the mesh near the triple line, where the more important concentration gradient are located.

Numerical solutions are obtained with the finite difference method using Stones's iteration method [9]. Finite-difference meshes used in calculations featured one node every 1° for $\varphi$ and 200 nodes for variable $\eta$. With 400 nodes along the $\eta$ direction, calculated concentration gradients differed by less than 0.3%; the above-defined discretization was thus deemed sufficiently fine and used in all calculations reported here.

## Specialization to Cu–Cr spreading on carbon: treatment of interfacial reaction kinetics

We now focus specifically on the system investigated here (and in Ref. [3]), namely liquid Cu–Cr alloy drops forming a continuous $Cr_7C_3$ reaction layer while spreading on a flat vitreous carbon substrate; the problem is sketched in more detail in Fig. 7. The problem at hand is relatively complex because it is a free boundary problem in which the solid and liquid diffusion problems are coupled: indeed, the rate of reaction along the liquid/solid interface will generally depend on the local solute concentration $C$ in the liquid, which is a priori unknown since it depends on solution of the diffusion problem described by Eqs. 2–6. We thus do not aim to provide a full simulation of the series of experiments reported here; rather, we simply aim to show that the presence of a finite solute flux to the interface behind the triple line caused by continued interfacial reaction can indeed explain the observed deviation of data from Eq. 1a. To this end, we decouple to some extent the solid and liquid diffusion problems and assume a priori that the interfacial reaction layer has the two-zone simplified structure that was described in Section "Introduction."

A quantitative description of the interfacial reaction kinetics is needed, since these govern the term d$e$/d$t$ in Eq. 5. This is generally not simple because the two problems are interrelated: the rate of reaction along the liquid/solid interface will generally depend on the local solute concentration $C$ in the liquid, which is a priori unknown since it depends on solution of the diffusion problem

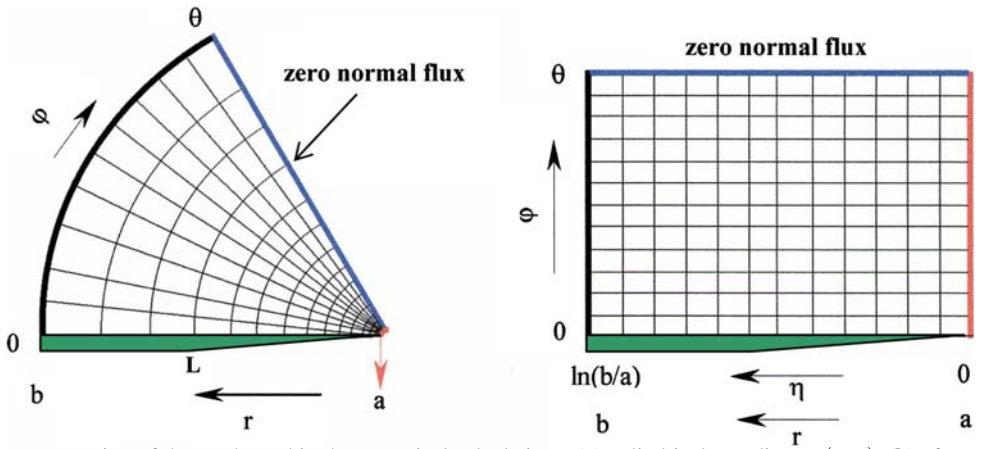


**Fig. 6** Schematic representation of the mesh used in the numerical calculations: (**a**) cylindrical coordinates $(r, \varphi)$, (**b**) after change of variables $(\eta, \varphi)$

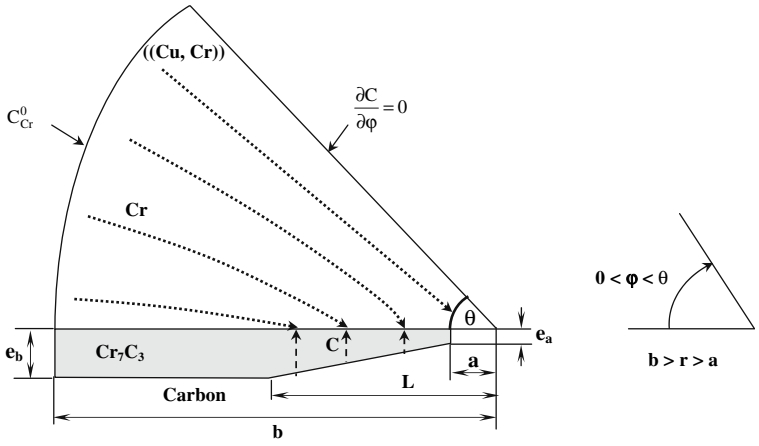


**Fig. 7** (**a**) Boundary conditions used to model the diffusion process, (**b**) cylindrical coordinate system

described by Eqs. 2–6. We therefore examine the specifics of chemical interaction between carbon and Cu–Cr alloys, stating the assumptions we make to ease tractability of the problem.

Based on the SEM characterization and microprobe analysis we consider that the only phase formed along the liquid/carbon interface is $Cr_7C_3$. The problem to be solved is, then, the diffusion-controlled growth of a layer $Cr_7C_3$ sandwiched between pure vitreous carbon and a liquid Cu–Cr alloy. This is sketched in Fig. 8.

Fries et al. [10] reported diffusion-controlled growth of carbide layers in the Cr–C system and showed that diffusion of chromium through chromium carbide is significantly slower than carbon diffusion. From this study we can conclude that reaction kinetics at the liquid/carbide interface are not rate-limiting and that growth of the $Cr_7C_3$ reaction layer occurs at the liquid/carbide interface.

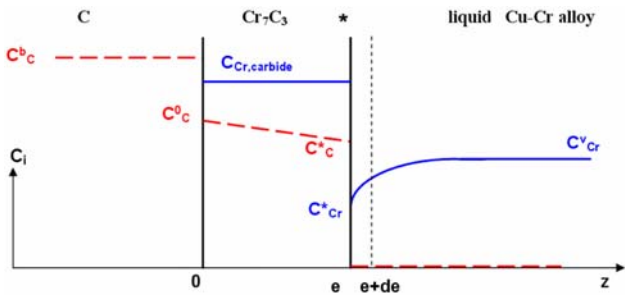


**Fig. 8** Schematic representation of Cr and C (*dotted line*) concentration profiles across the interfacial reaction layer in the Cu–Cr/C system. Solubility of C in liquid phase and of Cr in carbon are neglected. We assume stable local thermodynamic equilibrium at the liquid/carbide interface and metastable local equilibrium at the carbon/carbide interface. $C^b_C$ is the concentration of carbon in the bulk, $C^0_C$ and $C^*_C$ are the $Cr_7C_3$ carbon concentration at C/$Cr_7C_3$ and $Cr_7C_3$/liquid interfaces respectively. $C^v_{Cr}$ and $C^*_{Cr}$ are the liquid Cr concentrations in the drop volume and at the liquid/$Cr_7C_3$ interface, respectively

We assume that local thermodynamic equilibrium obtains along both interfaces: stable equilibrium at the liquid/carbide interface, and metastable equilibrium at the carbon/carbide interface, Fig. 8. Because of the very low carbon solubility in liquid Cu around 1,100 °C ( $< 10^{-7}$ at.% at 1,150 °C [11]), we ignore altogether the presence of carbon in the liquid. The carbide layer thickening rate then depends on: (i) the diffusion of chromium in the liquid from the drop bulk to the liquid/carbide interface (Eq. 5) and (ii) the diffusion of carbon in the solid reaction layer. Mass balance equations are expressed for chromium by Eqs. 5 and 11 and for carbon by Eq. 12:

$$\text{for chromium}: \quad \left(C_{\mathrm{Cr,carbide}} - C^*_{\mathrm{Cr}}\right)\frac{\mathrm{d}e}{\mathrm{d}t} = D\left(\frac{\partial C_{\mathrm{Cr}}}{r\partial\varphi}\right)_{e^+} \tag{11}$$

$$\text{for carbon}: \quad C^*_{\mathrm{C}}\frac{\mathrm{d}e}{\mathrm{d}t} = J_{\mathrm{C}}. \tag{12}$$

Thermodynamic equilibrium along the liquid Cu–Cr/$Cr_7C_3$ interface dictates:

$$\left(a^*_{\mathrm{Cr}}\right)^7\left(a^*_{\mathrm{C}}\right)^3 = \exp\left(\frac{\Delta G^0_{\mathrm{f}}(\mathrm{Cr_7C_3})}{RT}\right) \tag{13}$$

where $J_C$ is the diffusion flux of carbon through $Cr_7C_3$ (chromium diffusion is neglected), $a_{Cr}$ and $a_C$ are chromium and carbon chemical activity, respectively, $C_{Cr}$ and $C_C$ are chromium and carbon concentration, respectively, and $\Delta G^0_f(Cr_7C_3)$ is the molar standard free enthalpy of formation of $Cr_7C_3$ from liquid chromium and solid carbon. The asterisk superscript indicates that activities or concentrations are at the liquid/carbide interface, as indicated in Fig 8.

The diffusion flux of carbon in $Cr_7C_3$ carbide ($J_C$) is most conveniently expressed in terms of the chemical potential gradient $\mu_C$ [12]:

$$J_C \approx -\frac{x_C(1-x_C)D_C^*}{RTV_{Cr_7C_3}^m}\left(\frac{\partial \mu_C}{\partial z}\right)_{e^-} \quad (14)$$

where $V_{Cr_7C_3}^m$ is the molar volume of $Cr_7C_3$ ($m^3$ per mol of atoms), $x_C$ is the mean carbon content of $Cr_7C_3$ (nearly constant across the layer because of the narrow range of homogeneity), and $D_C^*$ is the self-diffusion coefficient of carbon in $Cr_7C_3$. Assuming a steady state (linear) profile for the carbon chemical potential across the carbide layer and using the classical expression ($\mu_C = \mu_C^0 + RT \ln a_C$), Eq. 14 can be rewritten as:

$$J_C \approx -\frac{x_C(1-x_C)D_C^*}{V_{Cr_7C_3}^m} \cdot \frac{\ln(a_C^*)}{e} \quad (15)$$

where $a_C^*$ is the carbon activity in carbide layer at the liquid/carbide interface (see Fig. 8) and $e$ the layer thickness. Therefore, Eq. 12 becomes (with $C_C^* = x_C/V_{Cr_7C_3}^m$) :

$$\frac{de}{dt} = -(1-x_C)D_C^*\frac{\ln(a_C^*)}{e}. \quad (16)$$

The rate of carbide layer thickening and the solute concentration profile in the liquid are, thus, interlinked problems. As was assumed in Section "Introduction," the reaction layer thickness profile near the triple line is taken to be linear between $r = a$ ($e = e_a$) and $r = L$ ($e = e_b$). From there until $r = b$, the reaction layer thickness is assumed to be constant (at $e = e_b$); see Fig. 7.

The diffusion coefficient of Cr in liquid Cu at 1,150 °C is taken as $D = 2 \times 10^{-9}$ $m^2$ $s^{-1}$ (typical of transition metals in copper at 1,373 K [13]). The average molar volume of atoms in the liquid is taken as $V_l^m = M_{Cu}/\rho_{Cu} = 7.94\,cm^3\,mol^{-1}$ and used to calculate the Cr concentration in liquid (mol $cm^{-3}$). The number of moles of reactive solute per unit volume of $Cr_7C_3$, $n_v$, is estimated at $7 \times \rho_{Cr_7C_3}/M_{Cr_7C_3} = 0.122$ mol $cm^{-3}$ [10, 14]; thus $V_{Cr_7C_3}^m = 5.76\,cm^3\,mol^{-1}$ of atoms. $\Delta G_f^0(Cr_7C_3) = -333880 + 50.846T$ J $mol^{-1}$ [15]. Henry's law is used, i.e., $a_{Cr} = \gamma_{Cr}^\infty x_{Cr}$, where $\gamma_{Cr}^\infty$ is the infinite dilution activity coefficient of Cr in liquid Cu referred to pure liquid Cr : $RT\ln\gamma_{Cr}^\infty = 81200 - 27.9T$ [16].

## Evaluation of parameters

We first evaluate parameters $L$ and $e_b$. As mentioned earlier, the most physically reasonable assumption is that growth of the reaction layer is solid-state diffusion-controlled and hence parabolic. The interfacial layer thickness $e$ is then given by:

$$e(\tau, R) = e_a + k[\tau(R)]^{1/2} \quad (17)$$

where $e_a$ is the thickness of the layer when it first forms at the triple line, $k$ is a kinetic constant and $\tau$ is the time of contact of the drop with the solid substrate at distance $R$ from the center of the drop ($\tau$ is obviously different from the spreading time $t$, these times being related through the spreading curves $R(t)$).

Assuming $e_a$ is negligible compared to the final thickness of the reaction layer (as will be seen below, this is consistent with data) observed values of the reaction layer thickness at the center of the drop, formed after some hundreds of seconds of contact, can be used to estimate an average value of the growth kinetic constant $k = 0.15$ μm $s^{-1/2}$ This value is in good agreement with the value of $k \approx 0.1\,\mu m\,s^{-1/2}$ obtained by Mortimer and Nicholas [17] who studied the interfacial reaction between a Cu–1% Cr alloy and vitreous carbon at 1,150 °C for reaction times as long as 4 h.

From Eq. 17 and the experimental data of variation with time of the drop base radius $R(t)$ and contact angle $\theta(t)$—cf. Fig. 2—we then calculate, for different spreading times (i.e., different contact angle values), the carbide layer thickness $e(R)$ as a function of distance $R$ from the center of the drop. Figure 9a presents such calculated curves $e(R)$, showing that the interfacial layer thickness at the center of the drop varies from about 0.5 μm ($t = 10$ s, $\theta = 83°$) to 1.5 μm at the end of spreading ($t = 100$ s, $\theta = 32°$). This figure clearly points out the contrast that exists, for a given time $t$, between the high rate of growth of the interfacial layer near the triple line and its much slower subsequent growth nearer the center of the drop. When time $t$ increases from 70 to 100 s and the triple line becomes almost immobile (displacements fall below 100 μm), the interfacial layer thickness increases by a factor 25 (from 0.04 to about 1 μm) whereas at the center of the drop the thickness of the layer increases only by 25% (from 1.2 to 1.5 μm). In other words, the rate of reaction is important only in a limited zone close to the triple line. These curves motivated the simplification made in modeling diffusion within the drop, namely taking the reaction layer thickness to increase linearly over a fixed distance $L$ from the triple line and remain constant thereafter; see Figs. 5d and 7.

To evaluate a mean value for $L$ we have plotted, for different spreading times, the variation of the diffusion flux $J$ through the layer at any point of the interface as a function of distance $R$ from the center of the drop, see Fig. 9b. We take $L$ as the region within which the diffusion flux is higher than 20% of $J_{max}$ (this value is somewhat arbitrary but captures well the width of the region of rapid diffusion). It can then easily deduced from Fig. 9b that $L$ varies from roughly 150 μm ($t = 10$ s, $\theta = 83°$) to 50 μm at the end of spreading ($t = 100$ s, $\theta = 32°$). In calculations

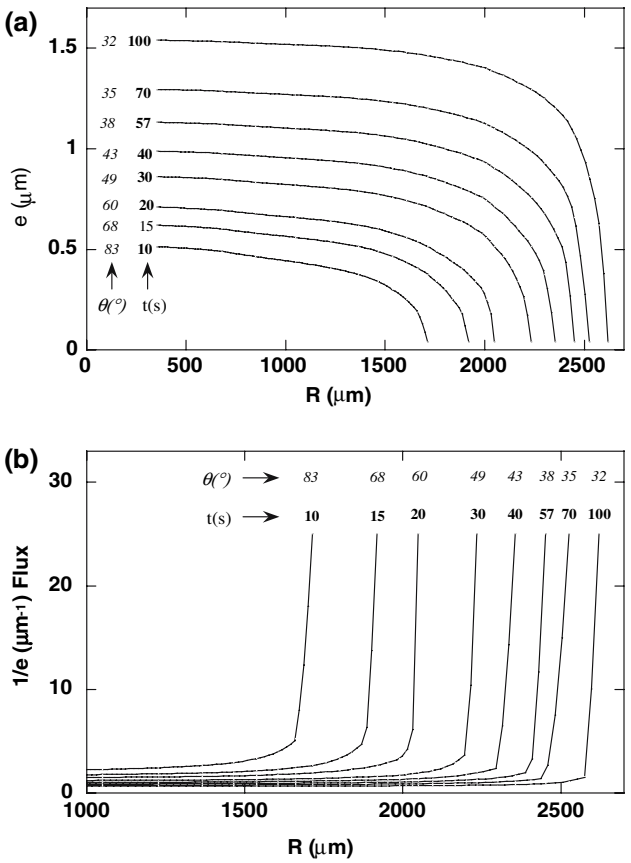


**Fig. 9** Variation with distance $R$ from the center of the drop of (**a**) the calculated carbide layer thickness $e$ and (**b**) carbon flux $J_C$ (in arbitrary units) through this layer at the Cu–1.5 at.% $Cr/C_V$ interface for different spreading times $t$ and contact angles $\theta$. $T$ = 1,150 °C. Values calculated according to Fig. 2 and Eq. 17 with $e_a$ = 40 nm and $k$ = 0.15 μm $s^{-1/2}$

we thus take the average value, of $L$ = 100 μm. Figure 9b indicates also that during spreading from $\theta = 83°$ to 32°, the reaction layer thickness increases from about 0.5 to 1.5 μm. As with $L$, we use the average value for the carbide layer thickness far from the triple line: $e_b$ = 1 μm.

Parameter $a$ is defined such that $(a{\cdot}\theta)$ is the linear area of the surface along which three-phase equilibrium obtains (between the Cu–Cr liquid alloy, vitreous carbon and $Cr_7C_3$, Fig. 8) [7]. This is expected to be on the order of a few nanometers; in the following calculations we have simply taken $a$ = 1 nm. According to Ref. [7], $b$ is then roughly $300\,\mu m \approx a\exp(1/0.08)$.

Two parameters in the equations system remain difficult to estimate: the initial thickness of carbide reaction layer formed at the triple line ($e_a$) and the self-diffusion coefficient of carbon across $Cr_7C_3$ ($D_C^*$).

If indeed the interpretation offered earlier, namely that continued reaction behind the triple line leaves the slope predicted by Eq. 1a unchanged, with all parameters other than the reaction layer known, this last parameter can be inferred from spreading kinetics at low angles, as was done in Ref. [3] (see the equation page 1125 of that reference). This gives $e_a$ = 40 nm for the present experiments.

An order of magnitude for $D_C^*$ can be gleaned from measurements of the growth kinetics of $Cr_7C_3$ during diffusion couple experiments. Fries et al. have performed such experiments with the carbon/chromium couple in the temperature range from 1,200 to 1,475 °C [10]. From their experiments and using a treatment as in Refs. [12, 18] we estimate $D_C^*$ to lie between $4\times\ 10^{-16}$ and $6\times\ 10^{-15}$ $m^2\ s^{-1}$. This range for the value of the self-diffusion coefficient of carbon through $Cr_7C_3$ is relatively wide because of: (i) dispersion in experimental data of Fries (extrapolated values for $(D_C\Delta C_C)$ where $\Delta C_C$ is poorly known (the range of $D_C\Delta C_C$ across $Cr_7C_3$ varies between $0.54\times\ 10^{-10}$ and $8.2\times\ 10^{-10}$ mol $m^{-1}\ s^{-1}$), and (ii) the fact that one must make assumptions in deducing $D_C^*$ from values of $D_C\Delta C_C$ (see Refs. [12] and [18]). We have therefore conducted calculations for several different values of $D_C^*$, using this single adjustable parameter as a measure of the relative importance of interfacial reaction behind the triple line. Parameters used in calculations are summarized in Table 1.

## Results of calculations and discussion

Results of numerical calculations for Cu–1.5 at.% Cr spreading on vitreous carbon at 1,150 °C with $e_a$ = 40 nm and for different values of the coefficient of diffusion through the reaction layer, $D_C^*$, values are plotted in Fig. 10. As seen, the precise value of $D_C^*$ in a realistic range of variation around the value $10^{-15}$ $m^2\ s^{-1}$ exerts a strong influence on the triple line velocity. If $D_C^* \le 10^{-16}\,m^2\,s^{-1}$, the rate of reaction product growth behind the triple line is negligible. The triple line velocity $V = dR/dt$ is then simply proportional to the instantaneous contact angle $\theta$, as predicted by the analytical model in Ref. [7] (Eq. 1), indicating thus the consistency of the numerical calculations in this limiting case. When $D_C^*$ increases above this value, the curve giving $V$ as a function of $\theta$ remains linear, retaining the same slope. The curve is, in other words, simply translated such that its intercept with the $\theta$-axis increases progressively with increasing $D_C^*$.

Under assumptions of the present model, therefore, the effect of continued interfacial reaction on spreading kinetics is indeed, as was surmised in Ref. [3], essentially to create a "dead-angle" in which all solute flux lines from the drop bulk are diverted away from the triple line to the liquid/solid interface, as was sketched in Fig. 11 of Ref. [3]. This "dead angle" $\theta_d$ appears simply in the data as the $\theta$-axis intercept of the straight line linking $V$ with $\theta$.

**Table 1** Summary of parameters used in diffusion analysis

| Parameter | | Value | Reference |
|---|---|---|---|
| Geometrical | $a$ | 1 nm | |
| | $b$ | 300 μm | |
| | $L$ | 100 μm | |
| | $e_a$ | 40 nm | |
| | $e_b$ | 1 μm | |
| | $\theta$ | 20° to 120° | |
| Thermodynamical | $\Delta G_f^0(Cr_7C_3)$ | –333880 + 50.846$T$ | [15] |
| | $RT \ln \gamma_{Cr}^{\infty}$ | 81200–27.9$T$ | [16] |
| Kinetical | $D_{Cr}$ (in liquid) | $2 \times 10^{-9}$ m$^2$ s$^{-1}$ | [13] |
| | $D_C^*$ (in $Cr_7C_3$) | $4 \times 10^{-16}$ to $6 \times 10^{-15}$ | [10, 12, 18] |
| Other | $V_{Cr_7C_3}^m$ | 5.76 cm$^3$ mol$^{-1}$ | [10, 14] |
| | $x_{Cr}$ | 0.015 | |

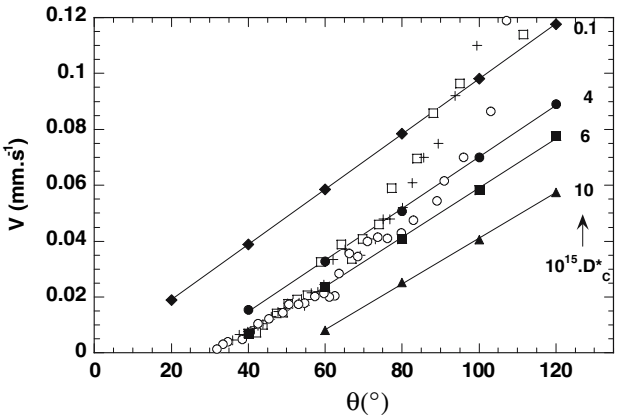


**Fig. 10** Experimental triple line velocity $V$(+, ○, □) and calculated values (◆, ●, ■, ▲) with $e_a$ = 40 nm as a function of instantaneous contact angle $\theta$ for various values of $D_C^*$ expressed as multiples of $10^{-15}$ m$^2$ s$^{-1}$, for Cu–1.50 at.% Cr spreading on flat vitreous carbon at 1,150 °C (calculations were conducted with $a$ = 1 nm, $b$ = 300 μm, $L$ = 100 μm and $e_b$ = 1 μm)

The experimental data are relatively well predicted for $D_C^* = 6 \times 10^{-15}$ m$^2$ s$^{-1}$ which, as mentioned above, is a realistic value [10]. Note that for a initial triple line reaction layer thickness values ($e_a$) that are high, i.e. some hundred of nanometres, the numerical calculations show that the values of diffusion coefficient in the carbide layer, susceptible to lead to a significant reactive solute flux behind the triple line, must be some orders of magnitude higher than $10^{-16}$ m$^2$ s$^{-1}$; this is unrealistic. Results thus indicate that either the initial carbide layer is less than 100 nm thick, or that alternatively this initial carbide layer is not dense, leading thus to a high cross-thickness diffusivity due to diffusion short-circuits. In this last case, of a porous carbide layer, the width of the boundary zone $L$ would be lower than the values of $L$ evaluated above (the higher the effective diffusivity through this layer is, the lower is the value of $L$).

Note also that for diffusion through titanium carbide at 1,020 °C, $D_C^*$ is less than $10^{-19}$ m$^2$ s$^{-1}$, which is well below the value $10^{-16}$ m$^2$ s$^{-1}$ [12]. The effect of interfacial reaction layer thickening behind the triple line is thus indeed expected to be negligible for Cu–15 at.% Sn–3 at.% Ti spreading on vitreous carbon, as observed [4].

Variations in the assumed geometrical parameters characterizing growth of the interfacial reaction layer in the model are explored in Fig. 11, where one can see the influence of variations in $L$ (Fig. 11a); $a$ (Fig. 11b) and $b$ (Fig. 11c). As seen, varying $L$ causes a shift in the curve, the slope of which remains constant. A decrease in $L$ thus causes a decrease in the effective dead-angle: this is to be expected, since a decrease in $L$ all else being constant will cause a decrease in the extent of solute flux diversion away from the triple line towards the interface. Most importantly, however, the influence of $L$ is relatively small: a 3-fold increase in $L$ has less effect than a doubling of $D_C^*$ (compare Figs. 10 and 11a).

In all cases, it is seen that the simulation yields the same general result: interfacial reactivity manifests itself by the presence of a finite "dead-angle" that must be subtracted from $\theta$ in Eq. 1a, this equation remaining otherwise essentially valid. The same result was found analytically in Ref. [3] for the extreme case of kinetically unhindered chemical reaction and very fast diffusion of the reactive species through the reaction layer.

Without providing a rigorous proof, the reason for this can in fact be relatively easily seen by examination of Fig. 6, especially Fig. 6b. Suppose indeed that, with a finite reaction rate along the interface, we consider solutions to the diffusion problem in Fig. 6b defined by Eqs. 3–6 and Eq. 10 starting from vanishingly small $\theta$. At vanishingly

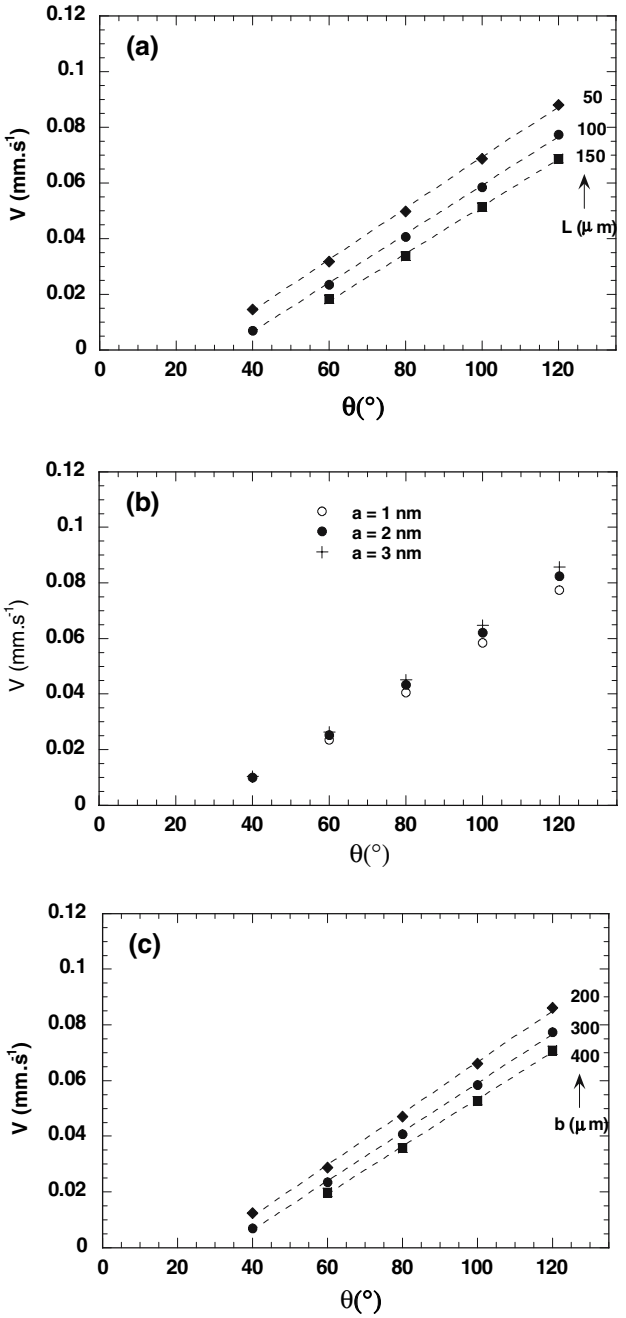


**Fig. 11** Calculated values of triple line velocity, for Cu–1.50 at.% Cr spreading on flat vitreous carbon at 1,150 °C, with $D_C^* = 6 \times 10^{-15}$ $m^2\ s^{-1}$, varying (**a**) $L$ from 50 to 150 μm, (**b**) $a$ from 1 to 3 nm, and (**c**) $b$ from 200 to 400 μm, with all other parameters as given in Table 1

small $\theta$, it is to be expected that no solute will reach the triple line, or in other words that essentially no flux line will span the entire length across the rectangle, from $\eta = ln\ (b/a)$ to $\eta = 0$. As $\theta$ increases, at some finite value of $\theta$, $\theta_d$, a first solute flux line will reach the triple line, i.e., go to $\eta = 0$ starting from the top left-hand corner at $\eta = ln\ (b/a)$ in the drawing of Fig. 6b. For values of $\theta$ higher than this, the solution to the problem will not be very different from the superposition of (i) the solution for $\theta = \theta_d$, and (ii) above this, the solution for $(\theta–\theta_d)$ with no interfacial reaction. Indeed, the boundary condition along the junction between these two solutions (the line $\theta = \theta_d$) is a no-flux boundary condition in both partial problems. Along this line, the solute distribution given by this superposition of two solutions will be altered somewhat to obey the Laplace equation (and also, the Laplace equation is not strictly valid for the problem at hand); however, it is likely that this will not alter extensively this approximate solution to the problem. In short, one may expect that the observed influence of continued interfacial reactivity behind the triple line on diffusion-limited spreading, namely the simple presence of a "dead-angle" subtracted to $\theta$ in Eq. 1a, to be rather general.

We finally note that, according to the present analysis, it is fortuitous that a zero spreading rate is reached very near the equilibrium contact angle for the melt on the reaction layer, $\theta_e$, in experimental plots of triple line velocity versus contact angle, Figs. 1 and 10. Had $D_C^*$ been somewhat lower or nil, spreading of the drop would stop abruptly upon reaching this equilibrium value. With higher values of $D_C^*$, on the other hand, rapid interfacial reaction would prevent the drop from reaching its final equilibrium contact angle on the reaction layer material because, once $\theta$ reaches $\theta_d$, further growth of the layer at the triple line is prevented by sustained interfacial reaction along the existing liquid/solid interface.

## Conclusion

Sessile drop experiments in the Cu–Cr/carbon system, conducted using the dispensed drop method followed with rapid cooldown, show the existence of a thickness gradient in the $Cr_7C_3$ carbide reaction layer along the interface. Spreading kinetics are consistent with prior work on this system. The carbide thickness gradient and the observed spreading kinetics of the drop both suggest that continued interfacial reaction occurs along the liquid/solid interface behind the triple line.

A finite-difference simulation of diffusion-limited reactive wetting in this system is conducted assuming a fixed and linear carbide thickness profile decreasing from 1 μm to 40 nm over the last 100 μm from the drop bulk to the triple line. Growth kinetics of the carbide, as limited by carbon diffusion from the substrate to a liquid/solid interface at local thermodynamic equilibrium, is modeled using the diffusivity of carbon through the carbide reaction layer as a measure of the relative importance of continued interfacial reaction of spreading kinetics. Results of the calculations predict well the observed spreading kinetics in

this system for a realistic value of the carbon diffusion coefficient $D_C^*$ equal to $6 \times 10^{-15}$ $m^2$ $s^{-1}$. This simplified but realistic simulation shows that the influence of continued reaction behind the triple line in diffusion-limited reactive wetting cause, in systems of the present class, the formation of a relatively constant "dead angle" $\theta_d$ in the liquid edge, across which solute diffusion is deviated away from the triple line. Spreading thus proceeds as predicted by Eq. 1a modified by substitution of the instantaneous contact angle $\theta$ with $(\theta–\theta_d)$.

**Acknowledgement** This work was supported by core funding at the respective authors' laboratories.

## References

1. Naidich YV (1981) In: Cadenhead DA, Danielli JF (eds) Progress in surface and membrane science, vol 14. Academic Press, New York, p 380
2. Eustathopoulos N, Nicholas MG, Drevet B (1999) Wettability at high temperatures. Elsevier, Kidlington, p 198, 317
3. Voitovitch R, Mortensen A, Hodaj F, Eustathopoulos N (1999) Acta Mater 47:1117
4. Dezellus O, Hodaj F, Mortensen A, Eustathopoulos N (2001) Scripta Mater 44:2543
5. Dezellus O, Hodaj F, Eustathopoulos N (2002) Acta Mater 50:4741
6. Landry K, Eustathopoulos N (1996) Acta Mater 44:3923
7. Mortensen A, Drevet B, Eustathopoulos N (1997) Scripta Mater 36:645
8. Carslaw HS, Jaeger JC (1959) Conduction of heat in solids, 2nd edn. Clarendon Press, Oxford, UK, pp 166–167, 431–434
9. Stone HL (1968) SIAM J Numer Anal 5:530
10. Fries RJ, Cummings JE, Hoffma CG, Daily SA (1967) US Atomic Energy Comm Report, LA-3795-MS. pp 1–32
11. Oden LL, Gokcen NA (1992) Met Trans B 23B:453
12. Van Loo FJJ, Bastin GF (1989) Metall Trans A 20A:403
13. Weast RC, Lide DR, Astle MJ, Beyer WH (1990) CRC handbook of chemistry and physics, 70th edn. CRC Press, Inc, Boca Raton, pp B-85, F-52
14. Nouveau traité de chimie minérale, Masson et Cie Editeurs. Tome XII, Paris (1959), p 367
15. Chase MW (ed) (1998) NIST JANAF Thermochemical Tables, 4th edn. American Society and American Institute of Physics for the National Institute of Standards and Technology. Monograph Nr. 9
16. Chakrabarti DJ, Laughlin DE (1984) Bull Alloy Phase Diagrams 5(1):59
17. Mortimer DA, Nicholas M (1973) J Mat Sci 8:640
18. Gülpen JH, Kodentsov AA, Van Loo FJJ (1995) Z Metallkunde 86:530